

## Gas phase UV and IR absorption spectra of $C_xF_{2x+1}CHO$ ( $x = 1-4$ )

Y. Hashikawa<sup>a</sup>, M. Kawasaki<sup>a</sup>, R.L. Waterland<sup>b,\*</sup>, M.D. Hurley<sup>d</sup>, J.C. Ball<sup>d</sup>,  
T.J. Wallington<sup>d</sup>, M.P. Sulbaek Andersen<sup>c</sup>, O.J. Nielsen<sup>c</sup>

<sup>a</sup>Department of Molecular Engineering and Graduate School of Global Environmental Studies, Kyoto University,  
Kyoto 615-8510, Japan

<sup>b</sup>DuPont Engineering Research and Technology, E. I. du Pont de Nemours and Co. Inc., P. O. Box 80249,  
Wilmington, DE 19880-0249, USA

<sup>c</sup>University of Copenhagen, Universitetsparken 5, DK-2100 Copenhagen, Denmark

<sup>d</sup>Ford Motor Company, P.O. Box 2053, Dearborn, MI 48121-2053, USA

Received 24 June 2004; received in revised form 21 July 2004; accepted 21 July 2004

Available online 11 September 2004

### Abstract

The UV and IR spectra of  $C_xF_{2x+1}CHO$  ( $x = 1-4$ ) were investigated using computational and experimental techniques.  $C_xF_{2x+1}CHO$  ( $x = 1-4$ ) have broad UV absorption features centered at 300–310 nm. The maximum absorption cross-section increases significantly and shifts slightly to the red with increased length of the  $C_xF_{2x+1}$  group:  $CF_3CHO$ ,  $3.10 \times 10^{-20}$  (300 nm);  $C_2F_5CHO$ ,  $6.25 \times 10^{-20}$  (308 nm);  $C_3F_7CHO$ ,  $8.96 \times 10^{-20}$  (309 nm); and  $C_4F_9CHO$ ,  $10.9 \times 10^{-20}$  (309 nm). IR spectra for  $C_xF_{2x+1}CHO$  were recorded, calculated, and assigned. Results are discussed with respect to the literature data and to the atmospheric fate of  $C_xF_{2x+1}CHO$ .

© 2004 Elsevier B.V. All rights reserved.

**Keywords:** Absorption spectra; PFOA; PFCA

### 1. Introduction

There is growing interest in the environmental fate and effects of fluorinated chemicals. Perfluorooctane sulfonate (PFOS,  $C_8F_{17}SO_3^-$ ) has been shown to be widely distributed in trace quantities in the Northern Hemisphere [1], and very recently, derivatives of perfluorooctanoic acid (PFOA,  $C_7F_{15}COOH$ ) and of other perfluoroalkyl carboxylic acids (PFCAs,  $C_xF_{2x+1}COOH$ , where  $x = 6-12$ ) have been observed in trace quantities in fish [2,3] and mammals [4] in remote locations.

The source of PFCA derivatives is unknown at present but several possibilities have been examined. Mabury and coworkers [5] have studied the thermolysis of fluoropolymers as a potential source of PFCAs in the environment. Recently, Yamada and Taylor [6] have studied the incineration of fluorinated acrylic polymers and fabric

blends treated with such polymers. Their study, which was conducted at conditions typical for municipal incinerators, concluded that no detectable levels of PFOA result from incineration of these fluorinated materials.

Fluorinated surfactants are commonly used as processing aids in the production of fluoropolymers and fluoroelastomers [7]. In most commercial processes, fluoropolymers are heated in excess of 350 °C to allow melt processing or sintering of the resin particles and it has been proposed that thermal degradation of residual surfactant during such processing could lead to PFCAs or their derivatives. However, a recent kinetic study of the thermal degradation of ammonium perfluorooctanoate (APFO,  $C_8F_{15}COO^-NH_4^+$ ), the carboxylate surfactant most commonly used as a processing aid, showed no evidence for production of PFOA [8].

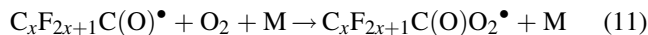
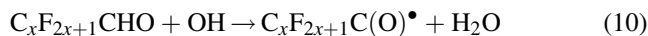
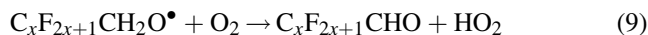
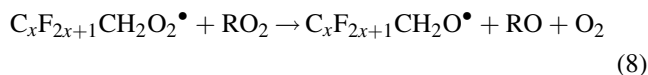
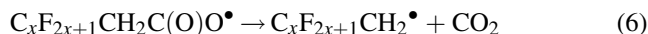
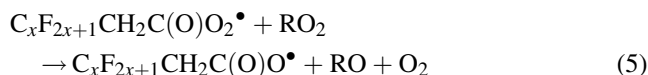
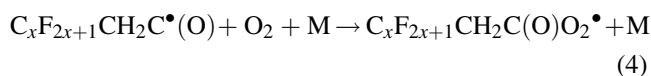
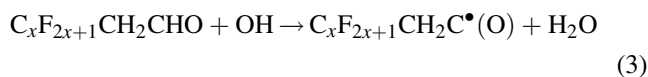
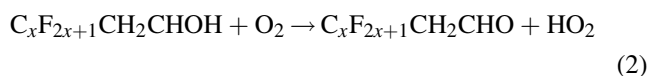
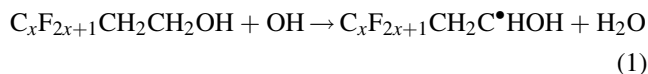
PFCAs observed in remote locations may arise from a variety of competing pathways including, but not limited to, atmospheric direct and indirect transport and poorly understood food chain processes. Much attention has

\* Corresponding author. Tel.: +1302 6951511; fax: +1 302 6958805.

E-mail addresses: [robert.l.waterland@usa.dupont.com](mailto:robert.l.waterland@usa.dupont.com) (R.L. Waterland), [twalling@ford.com](mailto:twalling@ford.com) (T.J. Wallington).

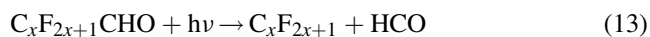
focussed on PFCA production from atmospheric degradation of precursor chemicals. Unfortunately, the identity of any atmospheric precursors and the mechanism by which they are converted into PFCAs are unclear at the present time.

Fluorotelomer alcohols, (FTOHs,  $C_xF_{2x+1}CH_2CH_2OH$ ) are chemical intermediates commonly used in the manufacture of fluorotelomer-based products. Although, the environmental fate of fluorotelomer-based substances is not fully determined, it has been suggested that atmospheric oxidation of FTOHs may be a source of PFCAs in the environment [9]. Sulbaek Andersen et al. [10] have proposed a three step mechanism. First, FTOHs react with OH radicals leading to formation of perfluorinated aldehydes. In the second step, OH radicals react with the newly-formed perfluorinated aldehydes to give perfluoroacetyl peroxy radicals,  $C_xF_{2x+1}C(O)O_2$ . Finally, reaction of  $C_xF_{2x+1}C(O)O_2$  with  $HO_2$  radicals produces PFCAs [10].



This mechanism will not be effective in air masses with high  $NO_x$  (e.g., urban areas) where loss of  $C_xF_{2x+1}C(O)O_2^{\bullet}$  will be dominated by reaction with  $NO_x$ . For the above mechanism to be a significant source of PFCAs, reaction with OH radicals (reaction 10) must be an important loss mechanism for  $C_xF_{2x+1}CHO$ . Photolysis is a likely alternate loss mechanism that will compete directly with reaction (10). Non-halogenated aldehydes absorb in the UV at 250–350 nm. It is well established that UV-induced C–C bond scission is an important atmospheric loss mechanism for aldehydes [11]. It seems reasonable to propose an analogous

photodissociation pathway as an atmospheric loss process for  $C_xF_{2x+1}CHO$ .



Photolysis via reaction will compete with reaction and suppress the formation of PFCAs by the mechanism described above. Two pieces of information are required to incorporate reaction (13) into models of the atmospheric chemistry of FTOHs and assess the importance of this process. First, we need the UV absorption spectra of  $C_xF_{2x+1}CHO$ . Second, we need photodissociation quantum yields for  $C_xF_{2x+1}CHO$  as a function of wavelength.

While the UV absorption spectrum of  $CF_3CHO$  has been measured in several studies [12–16] and is well defined, there is little information available concerning the UV absorption spectra of longer chain, and potentially environmentally more significant, perfluoroaldehydes. At the start of the present work there was no information available concerning the photodissociation quantum yields of  $C_xF_{2x+1}CHO$ . During the course of the present work, Sellevåg et al. [16] reported an upper limit of 0.02 for the effective photodissociation quantum yield of  $CF_3CHO$  in 1 atm of air with 290–400 nm radiation.

To facilitate the inclusion of reaction in atmospheric chemistry models and the experimental study of the atmospheric chemistry of  $C_xF_{2x+1}CHO$ , a computational and experimental study of the UV and IR spectra of  $C_xF_{2x+1}CHO$  ( $x = 1-4$ ) was performed in our laboratories. Results are reported herein. Straight chain isomers  $n-C_3F_7CHO$  and  $n-C_4F_9CHO$  were studied in the present work. For simplicity we will refer to these species as  $C_3F_7CHO$  and  $C_4F_9CHO$  in the rest of this article.

## 2. Experimental and computational details

Samples of  $C_xF_{2x+1}CHO$  ( $x = 1-4$ ), were synthesized from the corresponding hydrates  $C_xF_{2x+1}CH(OH)_2$  ( $x = 1-4$ ) using the procedure previously described for  $C_2F_5CHO$  [17]. The samples were purified by vacuum distillation.

### 2.1. UV measurements

UV absorption spectra of  $C_xF_{2x+1}CHO$  ( $x = 1-4$ ) were measured in the 200–500 nm wavelength range using a commercial dual beam UV spectrometer (Lambda 18, Perkin-Elmer) operated at a spectral resolution of 1.0 nm. Gaseous samples of  $C_xF_{2x+1}CHO$  were introduced using a Pyrex gas handling system with greaseless valves into a 5.8 cm long Pyrex cell equipped with  $BaF_2$  windows. Gas pressures were in the range 15–150 Torr as measured using with capacitance manometers (MKS). No diluent gas was added. All measurements were performed at 296 K. The purity of compounds was checked using FTIR spectroscopy before and after the UV measurements; no impurities were evident in the IR spectra.

## 2.2. IR measurements

The experimental setup consisted of a Mattson Instruments, Sirius 100 Fourier transform infrared spectrometer, interfaced to a 140 l, 2 m long evacuable Pyrex chamber described elsewhere [18]. The spectrometer was operated at a spectral resolution of  $0.50\text{ cm}^{-1}$ . Infrared spectra were derived from 32 co-added interferograms. Spectra were recorded at 296 K in the presence of 700 Torr of air diluent. We estimate the absorption cross-section measurement to be accurate to within  $\pm 5\%$  [18].

## 2.3. Computational details

Time-dependent density functional theory (TD-DFT) is rapidly becoming the standard method for rapid and accurate prediction of the properties of electronically excited states and for the estimation of UV and visible spectra. TD-DFT was first proposed by Ando [19] in the 1970s. Despite subsequent development and application to atoms [20–22] and solids [23,24], TD-DFT has only recently been applied to molecules. The first substantial molecular calculations were published in the mid to late 1990s [25,26]. Recently, a number of groups have used TD-DFT to predict UV and visible spectra for a broad array of molecular species [27–33] and in each of these studies, comparison of calculated and experimental transition energies showed that TD-DFT significantly outperforms older Hartree–Fock-based methods such as configuration interaction singles (CIS) [34]. Of particular importance for the present work, studies by Matsuzawa and co-workers [35] for about 40 molecules spanning a broad variety of fluorinated organics including ethers, aldehydes, acids and esters and Waterland et al. [36] for fluoroalkanes demonstrated that TD-DFT calculations of photoabsorption spectra, which incorporate empirical correction of the transition energy are very useful aids for molecular design.

In the present work, all calculations were performed using the Gaussian 03 suite of programs [37]. We used the gradient-corrected level of density-functional theory (DFT) utilizing Becke's three-parameter exchange functional [38] and the Lee–Yang–Parr correlation functional [39] (B3LYP).

Molecular geometries were optimized using the DFT-derived DZVP basis set [40] and the same basis set was used for frequency calculations to ensure that computed geometries corresponded to bound molecular states. Vertical excitation energies and oscillator strengths were calculated with time-dependent density-functional theory (TD-DFT) [25,41]. The TD-DFT calculations employed 50 states and used the DZVP basis set augmented with Dunning and Hay's Rydberg functions [42] on all heavy atom centers. We incorporated energy re-scaling in the same manner as Matsuzawa et al. [35] and Waterland et al. [36]. Our empirical fitting of the experimental spectra of formaldehyde,

benzene and methane gave the correlation

$$E_{\text{expt}} = 1.144 E_{\text{calc}} - 0.553\text{ eV}$$

with an  $R^2$  of 0.961.

For the estimation of IR spectra, we re-optimized all molecular geometries using B3LYP with the 6-31G\* basis set [43] and computed harmonic vibrational frequencies and intensities at the same level of theory on the resultant optimized geometries. Vibrational frequencies were scaled by 0.961 as recommended by Scott and Radom [44].

## 3. Results

### 3.1. Measured UV spectra

As an initial control experiment, the UV spectrum of  $\text{CH}_3\text{CHO}$  was measured using the same techniques and apparatus used to study  $\text{C}_x\text{F}_{2x+1}\text{CHO}$ . The spectrum of  $\text{CH}_3\text{CHO}$  measured in the present work (solid trace) is compared to the recommended literature spectrum [45] (circles) in the bottom panel of Fig. 1. The excellent agreement between the spectrum of  $\text{CH}_3\text{CHO}$  measured in

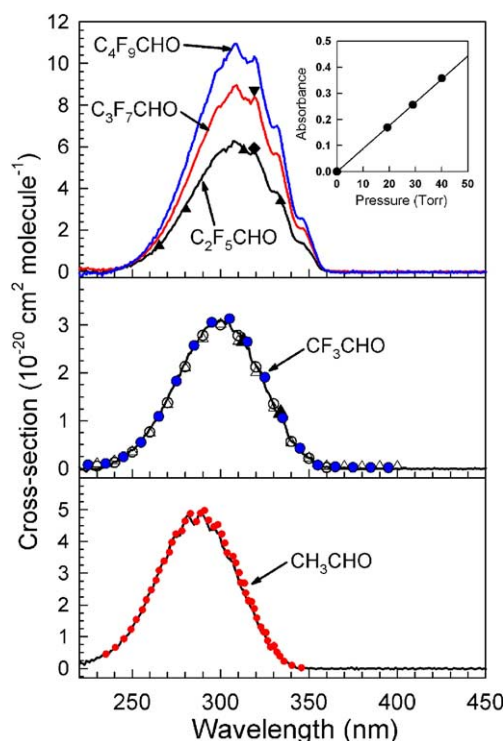


Fig. 1. UV spectra for  $\text{CH}_3\text{CHO}$  (bottom panel),  $\text{CF}_3\text{CHO}$  (middle panel) and  $\text{C}_2\text{F}_5\text{CHO}$ ,  $\text{C}_3\text{F}_7\text{CHO}$ , and  $\text{C}_4\text{F}_9\text{CHO}$  (upper panel) recorded in the present work (solid traces). The circles in the lower panel are the spectrum of  $\text{CH}_3\text{CHO}$  recommended by Nölle et al. [45]. The filled triangles, open triangles, open circles, and blue circles in the middle panel are the data for  $\text{CF}_3\text{CHO}$  from Borkowski and Ausloos [12], Francisco and Williams [14], Meller et al. [13], and Sellevåg et al. [16], respectively. Triangles and diamond in the top panel are data for  $\text{C}_2\text{F}_5\text{CHO}$  from Borkowski and Ausloos [12] and Pritchard et al. [46], respectively. The inverted open triangle is a datum for  $\text{C}_3\text{F}_7\text{CHO}$  from Pritchard et al. [46].

the present work and the literature data provides confidence in our experimental methodology.

UV spectra of  $C_xF_{2x+1}CHO$  ( $x = 1-4$ ) were measured over the wavelength range 200–500 nm. The UV spectra of at least three samples of each gas were measured as a check of both experimental reproducibility and linearity of absorption with reagent concentration. The insert in the top panel of Fig. 1 shows the observed absorbance at 309 nm as a function of the concentration of  $C_4F_9CHO$  and serves to illustrate the typical linearity and reproducibility observed during the present work. Linear least squares analysis of the data in the insert gives a value of  $\sigma(309 \text{ nm}, C_4F_9CHO) = 1.09 \times 10^{-19} \text{ cm}^2 \text{ mol}^{-1}$ . As indicated by the data in the insert in Fig. 1, the measurements were reproducible to within  $\pm 3\%$ . We estimate that systematic uncertainties associated with the pressure and path length measurements add an additional 5% uncertainty to give a final value of  $\sigma(309 \text{ nm}, C_4F_9CHO) = (1.09 \pm 0.06) \times 10^{-19} \text{ cm}^2 \text{ mol}^{-1}$ . This value was used as a scaling point to derive the UV spectrum of  $C_4F_9CHO$  shown in the top panel of Fig. 1. The spectra of  $CF_3CHO$ ,  $C_2F_5CHO$ , and  $C_3F_7CHO$  shown in Fig. 1 were derived in a similar fashion. As seen from Fig. 1, the maximum absorption cross-section increases significantly and shifts slightly to the red with increased length of the  $C_xF_{2x+1}$  group:  $CF_3CHO$ ,  $(3.10 \pm 0.18) \times 10^{-20}$  (300 nm);  $C_2F_5CHO$ ,  $(6.25 \pm 0.36) \times 10^{-20}$  (308 nm);  $C_3F_7CHO$ ,  $(8.96 \pm 0.52) \times 10^{-20}$  (309 nm); and  $C_4F_9CHO$ ,  $(10.9 \pm 0.6) \times 10^{-20}$  (309 nm). Spectral data for  $C_xF_{2x+1}CHO$  ( $x = 1-4$ ) at 10 nm intervals are given in Table 1.

As shown in Fig. 1, our spectrum for  $CF_3CHO$  agrees well with the previous measurements by Borkowski and Ausloos [12], Francisco and Williams [14], Meller et al. [15], and Sellevåg et al. [16]. The spectrum for  $CF_3CHO$  reported by Lucazeau and Sandorfy [13] is similar in shape to that measured herein but is approximately 30% less intense. In light of the excellent agreement between the spectral data reported herein and by Borkowski and Ausloos [12], Francisco and Williams [14], Meller et al. [13], and Sellevåg et al. [16] it would appear that Lucazeau and Sandorfy [13] underestimated the absorption of  $CF_3CHO$  by approximately 30%.

Table 1  
Absorption cross-sections ( $10^{-20} \text{ cm}^2 \text{ mol}^{-1}$ ) measured in the present work

Wavelength (nm)	$CF_3CHO$	$C_2F_5CHO$	$C_3F_7CHO$	$C_4F_9CHO$
250	0.38	0.31	0.42	0.42
260	0.84	0.86	1.08	1.35
270	1.46	1.78	2.39	2.89
280	2.20	3.13	4.16	5.01
290	2.86	4.64	6.24	7.63
300	3.01	5.75	7.91	9.75
310	2.83	6.14	8.76	10.74
320	2.15	5.66	8.32	10.22
330	1.33	3.84	5.62	6.92
340	0.57	1.94	2.94	3.56
350	0.22	1.01	1.56	1.82

As seen from the top panel of Fig. 1, the spectra of  $C_2F_5CHO$  and  $C_3F_7CHO$  measured in the present work are in good agreement with the absorption cross-sections reported by Borkowski and Ausloos [12], and Pritchard et al. [46] for these species. There are no literature data for  $C_4F_9CHO$  with which we can compare our results.

### 3.2. Measured IR spectra

IR spectra of  $C_xF_{2x+1}CHO$  ( $x = 1-4$ ) measured in the present work are shown in Fig. 2. As seen from the bottom panel the measurements in the present work are in excellent agreement with the previous work by Sellevåg et al. [16]. Integrated absorption intensities over the wavenumber range 670–3000  $\text{cm}^{-1}$  measured in the present work were  $S = 1.30, 1.67, 1.97,$  and  $2.29 \times 10^{-16} \text{ cm mol}^{-1}$  for  $CF_3CHO, C_2F_5CHO, C_3F_7CHO,$  and  $C_4F_9CHO$ , respectively. Francisco and Williams [14] have reported integrated absorption intensities over the range 801–2890  $\text{cm}^{-1}$  for  $CF_3CHO$  of  $2.7 \times 10^{-17}$  for pure vapor and  $1.07 \times 10^{-16} \text{ cm mol}^{-1}$  in the presence of 150–750 Torr of argon diluent. Sellevåg et al.

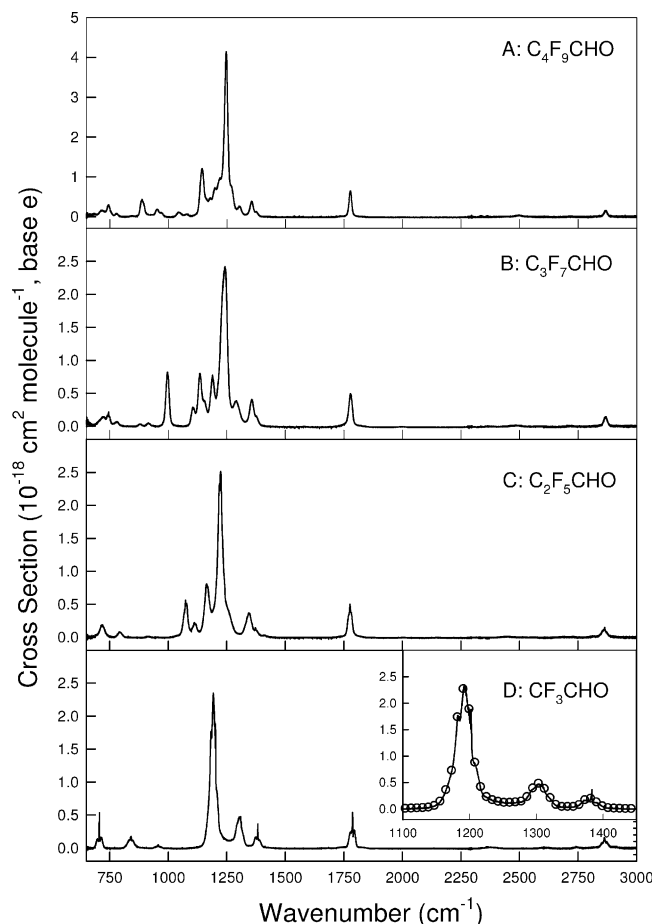
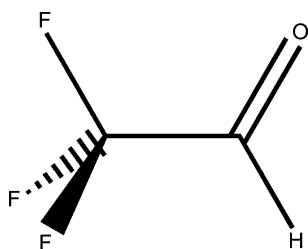


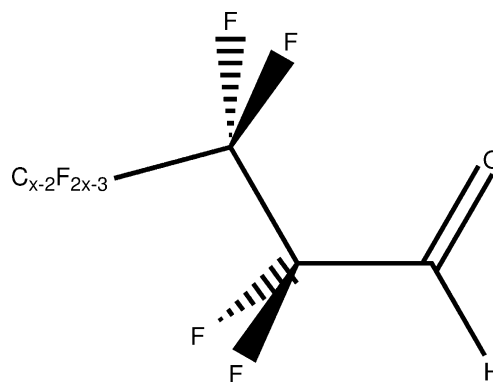
Fig. 2. IR spectra measured in the present work for  $C_xF_{2x+1}CHO$ . The insert in panel D shows a comparison of the spectrum for  $CF_3CHO$  reported by Sellevåg et al. [16] (circles) and that measured in the present work (solid trace).

Fig. 3. Lowest energy conformation of CF<sub>3</sub>CHO.

[16] report an integrated absorption intensity over the wavenumber range 775–3000 cm<sup>-1</sup> of  $S = 1.274 \times 10^{-16}$  cm mol<sup>-1</sup> for pure CF<sub>3</sub>CHO vapor. As seen from Fig. 2, there is a small absorption feature centered at 706 cm<sup>-1</sup> which was not recorded by either Francisco and Williams [14] or Sellevåg et al. [16]. Exclusion of absorption from this feature gives a value of  $S = 1.25 \times 10^{-16}$  cm mol<sup>-1</sup> at 800–3000 cm<sup>-1</sup> in the present work. This value is in excellent agreement with the previous work by Sellevåg et al. [16] and in fair agreement (15% discrepancy) with that reported by Francisco and Williams [14] in 150–750 Torr of argon diluent. The simplest explanation for the anomalously low absorption observed by Francisco and Williams [14] in the absence of diluent gas is saturation of the CF<sub>3</sub>CHO absorption features in their low pressure experiments.

### 3.3. Calculated UV spectra

Before we measured the UV spectra of C<sub>x</sub>F<sub>2x+1</sub>CHO ( $x = 1-4$ ), we first calculated them to guide the subsequent experimental measurements. Our first task was to determine the lowest energy molecular conformers for each of the four perfluoroalkyl aldehydes. As sketched in Fig. 3, the lowest energy conformation of CF<sub>3</sub>CHO has C<sub>s</sub> symmetry with the carbonyl oxygen eclipsing one of the C–F bonds. The ground electronic state is <sup>1</sup>A'. Energetically preferred

Fig. 4. Lowest energy conformer of C<sub>x</sub>F<sub>2x+1</sub>CHO ( $x = 2,4$ ).

conformers of the higher aldehydes, C<sub>x</sub>F<sub>2x+1</sub>CHO ( $x = 2,4$ ), have the carbonyl oxygen eclipsing the C–C single bond of the first tetrafluoroethylene segment. These conformations are sketched in Fig. 4. C<sub>2</sub>F<sub>5</sub>CHO and C<sub>3</sub>F<sub>7</sub>CHO have C<sub>s</sub> symmetry with ground electronic state <sup>1</sup>A' but, for C<sub>4</sub>F<sub>9</sub>CHO the perfluorinated develops a helical structure and the symmetry is lowered to C<sub>1</sub>. The ground electronic state of C<sub>4</sub>F<sub>9</sub>CHO is <sup>1</sup>A.

In Table 2 we show the wavelength and oscillator strength for the first 12 electronic transitions (singlet or triplet) in each of the perfluoroalkyl aldehydes studied. These transitions include all those with wavelengths greater than 150 nm. Since, the solar spectrum below 290 nm is completely blocked by stratospheric trace gases, a necessary condition for photolysis in the lower atmosphere is that the compound absorb UV at wavelengths above 290 nm. We have included lower wavelengths for completeness.

Singlet–triplet transitions are spin-forbidden and are marked with an 'f' in Table 2. We would not expect any intensity from these transitions in the experimental spectra. More surprisingly, in the critical wavelengths above 290 nm, all of the singlet–singlet transitions have oscillator strength less than or equal to 0.0001, i.e. they are predicted to be

Table 2  
Computed singlet and triplet transitions for C<sub>x</sub>F<sub>2x+1</sub>CHO ( $x = 1-4$ )

CF <sub>3</sub> CHO (C <sub>s</sub> / <sup>1</sup> A')			C <sub>2</sub> F <sub>5</sub> CHO (C <sub>s</sub> / <sup>1</sup> A')			C <sub>3</sub> F <sub>7</sub> CHO (C <sub>s</sub> / <sup>1</sup> A')			C <sub>4</sub> F <sub>9</sub> CHO (C <sub>1</sub> / <sup>1</sup> A)		
Upper state	λ <sub>calc</sub> (nm)	Oscillatory strength	Upper state	λ <sub>calc</sub> (nm)	Oscillatory strength	Upper state	λ <sub>calc</sub> (nm)	Oscillatory strength	Upper state	λ <sub>calc</sub> (nm)	Oscillatory strength
<sup>3</sup> A''	374.7	f	<sup>3</sup> A''	380.1	f	<sup>3</sup> A''	380.4	f	<sup>3</sup> A	380.6	f
<sup>1</sup> A''	300.4	<0.0001	<sup>1</sup> A''	305.2	<0.0001	<sup>1</sup> A''	306.1	<0.0001	<sup>1</sup> A	306.5	0.0001
<sup>3</sup> A'	219.6	f	<sup>3</sup> A'	220.0	f	<sup>3</sup> A'	219.5	f	<sup>3</sup> A	219.7	f
<sup>3</sup> A''	156.3	f	<sup>3</sup> A''	167.2	f	<sup>3</sup> A''	172.4	f	<sup>3</sup> A	177.7	f
<sup>3</sup> A'	156.2	f	<sup>1</sup> A''	159.8	0.0005	<sup>1</sup> A''	166.9	0.0001	<sup>1</sup> A	172.2	0.0005
<sup>1</sup> A'	153.8	0.0155	<sup>3</sup> A'	155.2	f	<sup>3</sup> A'	160.2	f	<sup>3</sup> A	164.8	f
<sup>3</sup> A'	143.0	f	<sup>1</sup> A'	152.2	0.0238	<sup>1</sup> A'	155.3	0.0408	<sup>1</sup> A	158.8	0.0608
<sup>3</sup> A'	140.5	0.0307	<sup>3</sup> A''	150.4	f	<sup>3</sup> A''	152.9	f	<sup>3</sup> A	154.0	f
<sup>3</sup> A'	140.2	f	<sup>3</sup> A'	146.6	f	<sup>3</sup> A'	150.1	f	<sup>3</sup> A	153.0	f
<sup>1</sup> A''	140.2	0.0017	<sup>1</sup> A'	143.7	0.0041	<sup>1</sup> A'	147.4	0.0038	<sup>1</sup> A	151.9	0.0052
<sup>1</sup> A'	140.1	0.0118	<sup>1</sup> A'	142.5	0.0371	<sup>1</sup> A''	147.0	0.0002	<sup>1</sup> A	151.5	0.0643
<sup>1</sup> A'	139.7	0.0030	<sup>1</sup> A''	140.6	0.0004	<sup>1</sup> A'	145.4	0.0135	<sup>1</sup> A	150.1	0.0001

Table 3

Observed and calculated vibrational bands ( $\text{cm}^{-1}$ ), calculated infrared intensities ( $\text{km mole}^{-1}$ ), and approximate band assignments for  $\text{C}_x\text{F}_{2x+1}\text{CHO}$ 

$\text{CF}_3\text{CHO}$			$\text{C}_2\text{F}_5\text{CHO}$			$\text{C}_3\text{F}_7\text{CHO}$			$\text{C}_4\text{F}_9\text{CHO}$			Approximate assignment
$\nu_{\text{obs}}$	$\nu_{\text{calc}}$	IR intensity	$\nu_{\text{obs}}$	$\nu_{\text{calc}}$	IR intensity	$\nu_{\text{obs}}$	$\nu_{\text{calc}}$	IR intensity	$\nu_{\text{obs}}$	$\nu_{\text{calc}}$	IR intensity	
706	673	34.4	718	664	18.4	745	725	7.2	745	717	19.7	
841	815	38.0	794	741	2.7	996	965	70.1	888	934	5.99	
			1074	1084	116.5	1104	1116	174.6		1117	172.5	
			1112	1136	155.6	1135 <sup>a</sup>	1144	88.4	1144	1149 <sup>a</sup>	42.5	Backbone bend <sup>b</sup>
			1164	1163	168.9	1189	1174	112.3		1178	186.5	
1192	1168 <sup>a</sup>	459.7	1224	1209	378.2	1243	1216 <sup>a</sup>	618.7	1247	1220	407.6	Backbone bend <sup>b</sup>
1303	1275	136.6		1303	83.6		1311	68.1		1310	90.9	C–C stretch
1383	1367	35.0	1345	1385	10.8	1357	1373	16.4	1357	1374	6.6	C–C–H bend
1787	1798	84.7	1776	1793	99.5	1778	1795	98.4	1778	1794	102.8	C=O stretch
2863	2870	60.3	2864	2857	61.2	2868	2852	63.7	2868	2851	65.6	C–H stretch

<sup>a</sup> Superposition of two or more bands:  $\nu_{\text{calc}}$  is set to the mean frequency and intensity is set to sum of individual band intensities.<sup>b</sup> Out of plane vibrational mode.

weak. Strong absorption is predicted to occur at wavelengths below 290 nm. For example,  $\text{CF}_3\text{CHO}$  has a strong singlet–singlet transition at 153.8 nm.

Similar behavior has been reported for formaldehyde. Experimentally, the UV spectrum of formaldehyde has a single broad absorption peak centered at 326 nm [47]. For this transition, the upper state is designated  $^1\text{A}_2(n,\pi^*)$  [48] and, under electric dipole rules, it is actually forbidden. That this transition is, in fact, experimentally observed is due to vibronic interaction as discussed by Dieke and Kistiakowski [49]. Calculation of the vibronic structure of molecules as large as those that are the focus of this study is not feasible at present but as a check, we calculated an UV spectrum for formaldehyde using the same method described above. The calculated spectrum has one singlet–singlet transition at 319 nm in good agreement with experiment but, in concordance with the fluorinated analogue, this transition has oscillator strength less than 0.0001. By analogy, although we cannot be certain, we think it likely that the low intensity singlet–singlet transitions shown in Table 2 correspond, in fact, to experimentally observable transitions.

In summary, the ab initio calculations identify the predicted spectral peak locations and how these peaks shift as the perfluorinated chain lengthens but do not give the relative peak intensity. For the fluoraldehydes, Table 2 shows that only one peak is predicted above 290 nm. The peak location shifts slightly to the red as the perfluorinated chain lengthens. The largest change is from  $\text{CF}_3\text{CHO}$  (300 nm) to  $\text{C}_2\text{F}_5\text{CHO}$  (305 nm) but slight additional red shifts occur for  $\text{C}_3\text{F}_7\text{CHO}$  (306 nm) and  $\text{C}_4\text{F}_9\text{CHO}$  (307 nm).

### 3.4. Calculated IR spectra

The calculation of vibrational normal modes and the corresponding harmonic vibrational frequencies is a routine operation for modern ab initio methods. In this work, we have followed the recommendation of Scott and Radom [44]. This method gave a root mean square error of  $34 \text{ cm}^{-1}$  for a set of 122 molecules and 1066 experimental vibrational frequencies.

Table 3 shows the experimentally observed vibrational bands and the corresponding computed vibrational counterparts. Theory and experiment agree well for the location of the bands. Taking all four molecules together, for those transitions for which both experimental and theoretical data exist, the root mean square error is  $24 \text{ cm}^{-1}$  and the maximum absolute error is  $54 \text{ cm}^{-1}$  which are typical for this level of theoretical treatment. Examining the molecules individually, the root mean square and maximum absolute errors are respectively, 18 and  $33 \text{ cm}^{-1}$  for  $\text{CF}_3\text{CHO}$ , 32 and  $54 \text{ cm}^{-1}$  for  $\text{C}_2\text{F}_5\text{CHO}$ , 17 and  $27 \text{ cm}^{-1}$  for  $\text{C}_3\text{F}_7\text{CHO}$ , and 27 and  $46 \text{ cm}^{-1}$  for  $\text{C}_4\text{F}_9\text{CHO}$ . Theoretical predictions show a modest systematic error for the highest intensity peaks. However, examination of the three most intense peaks for each molecule shows that the largest error is  $28 \text{ cm}^{-1}$ . The relative computed IR intensities also agree quite well with experiment. Fig. 5 shows the computed spectrum of  $\text{CF}_3\text{CHO}$  in the region  $1100\text{--}1500 \text{ cm}^{-1}$ . The theoretical spectrum has been artificially broadened to allow comparison with the corresponding experimental spectrum in Fig. 2D. The tendency to underpredict peak location is seen here

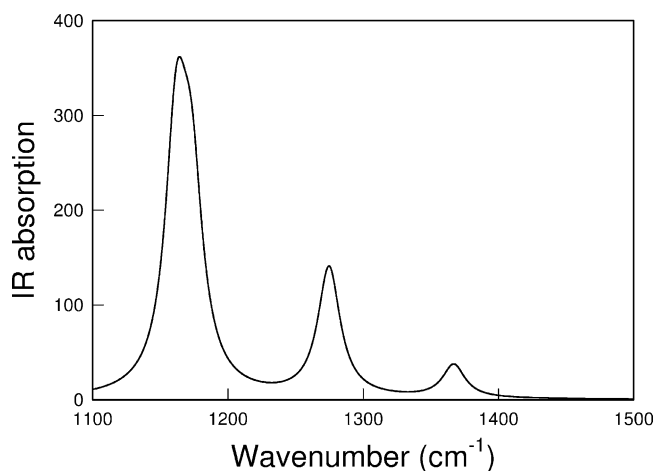


Fig. 5. Computed IR spectrum of  $\text{CF}_3\text{CHO}$ . The lines have been artificially broadened with a Lorentzian lineshape (full width at half maximum of  $20 \text{ cm}^{-1}$ ) for comparison with Fig. 2D.

but the relative intensity of the three strong peaks is well reproduced.

By visual inspection of each computed normal mode, we have attempted to describe the character of the modes in terms of stretching and bending deformations. These descriptions are approximate and the true normal modes usually involve a complicated mixture of atomic motions.

#### 4. Discussion

Our theoretical and experimental investigations show impressive agreement and lead us to several important conclusions. We have established that the perfluoroalkyl aldehydes  $C_xF_{2x+1}CHO$  ( $x = 1-4$ ), absorb strongly in the critical UV region above 290 nm. The absorption is concentrated in a broad single band and, for the higher aldehydes ( $x = 3,4$ ), the peak absorption is at 309 nm. We anticipate that the higher homologues  $C_xF_{2x+1}CHO$  ( $x > 4$ ), will absorb at a very similar wavelength.

The maximum in the absorption cross-section increases monotonically and rapidly with increasing length of the perfluorinated tail but we cannot say if this trend will hold for  $n > 4$ . The peak absorption of  $C_4F_9CHO$  is about 3.5 times greater than that of  $CF_3CHO$ .

The higher perfluoroalkyl aldehydes absorb more strongly than their corresponding non-halogenated counterparts [50]. Propionaldehyde has a peak absorption of  $5.88 \times 10^{-20}$  compared to  $6.25 \times 10^{-20}$  for  $C_2F_5CHO$  while the absorption cross-section for *n*-butyraldehyde peaks at  $6.17 \times 10^{-20}$  compared to  $8.96 \times 10^{-20} \text{ cm}^2 \text{ mol}^{-1}$  for  $C_3F_7CHO$ .

In addition, the non-halogenated aldehydes have their peak absorption much closer to the critical 290 nm threshold. The acetaldehyde cross-section peaks at 290 nm, propionaldehyde at 293 nm and *n*-butyraldehyde at 294 nm. This is important because the UV flux at the earth's surface increases rapidly as a function of wavelength for  $\lambda > 290$  nm. For a solar zenith angle of  $0^\circ$ , the UV flux at 309 nm is about 1400 times that at 294 nm [51]. Thus, we may safely conclude that absorption of solar UV in the lower atmosphere will be substantially greater for the perfluoroalkyl aldehydes as compared to their non-halogenated counterparts.

It is well established that the normal aldehydes,  $C_xH_{2x+1}CHO$ , undergo UV-induced C–C bond scission with quantum yields at 300 nm in the range 0.4–1.0 for  $x = 1-3$  [11]. For an altitude of 0.5 km and solar zenith angle of  $0^\circ$  it has been calculated that HCHO,  $CH_3CHO$ , and  $C_2H_5CHO$  photolyze at rates of  $1 \times 10^{-4}$ ,  $7 \times 10^{-6}$ , and  $2.5 \times 10^{-5} \text{ s}^{-1}$ , respectively [11]. Photolysis is an important loss atmospheric mechanism for normal aldehydes,  $C_xH_{2x+1}CHO$ . While, Sellevåg et al. [16] have reported an upper limit of 0.02 for the photolysis quantum yield of  $CF_3CHO$ , no data are available for longer chain perfluor-

oalkyl aldehydes,  $C_xF_{2x+1}CHO$ , and it is not possible to calculate their photolysis rate at this time.

As noted above, it is clear that absorption of solar UV in the lower atmosphere will be substantially greater for the perfluoroaldehydes than their non-halogenated analogues. However, in the absence of quantum yield data it is unclear whether the rate of photolysis of long chain perfluoroaldehydes is greater than, comparable to, or less than that of the corresponding normal aldehydes. Studies of the photolysis quantum yields for  $C_xF_{2x+1}CHO$  ( $x > 1$ ) under atmospheric conditions are needed to quantify the degree to which reaction (13) competes with reaction (10) and hence suppresses, and perhaps eliminates, formation of perfluorocarboxylic acids via the  $C_xF_{2x+1}C(O)O_2 + HO_2$  reaction.

#### Acknowledgements

Ole John Nielsen thanks the Danish Natural Science Research Council for financial support. In addition, we thank Robert C. Buck, Paul J. Krusic and Mary A. Kaiser for their critical review of the manuscript.

#### References

- [1] J.P. Giesy, K. Kannan, *Environ. Sci. Tech.* 35 (2001) 39.
- [2] C.A. Moody, J.W. Martin, W.C. Kwan, D.C.G. Muir, S.A. Mabury, *Environ. Sci. Tech.* 36 (2002) 545.
- [3] C.A. Moody, W.C. Kwan, J.W. Martin, D.C.G. Muir, S.A. Mabury, *Anal. Chem.* 73 (2001) 2200.
- [4] J.W. Martin, M.M. Smithwick, B.M. Braune, P.F. Hoekstra, D.C.G. Muir, S.A. Mabury, *Environ. Sci. Tech.* 38 (2004) 373.
- [5] D.A. Ellis, S.A. Mabury, J.W. Martin, D.C.G. Muir, *Nature* 412 (2001) 6844.
- [6] P. Taylor, T. Yamada, R. Giraud, M. Kaiser, R. Buck, *Environ. Sci. Tech.*, in press.
- [7] E. Kissa, *Fluorinated surfactants and repellents*, in: *Surfactant Science Series*, Marcel Dekker, New York, 2001.
- [8] P.J. Krusic, D.C. Roe, *Anal. Chem.* 76 (2004) 3800.
- [9] D.A. Ellis, J.W. Martin, A.O. De Silva, S.A. Mabury, M.D. Hurley, M.P. Sulbaek Andersen, T.J. Wallington, *Environ. Sci. Tech.* 38 (2004) 3316.
- [10] M.P. Sulbaek Andersen, M.D. Hurley, T.J. Wallington, J.C. Ball, J.W. Martin, D.A. Ellis, S.A. Mabury, *Chem. Phys. Lett.* 381 (2003) 14.
- [11] J.G. Calvert, R. Atkinson, J.A. Kerr, S. Madronich, G.K. Moortgat, T.J. Wallington, G. Yarwood, *Mechanisms of the Atmospheric Oxidation of the Alkenes*, Oxford, University Press, 2000, ISBN: 0-19-513177-0.
- [12] R.P. Borkowski, P. Ausloss, *J. Am. Chem. Soc.* 84 (1962).
- [13] G. Lucazeau, C. Sandorfy, *J. Mol. Spectrosc.* 35 (1970) 14.
- [14] J.S. Francisco, I.H. Williams, *Mol. Phys.* 6 (1992) 1433.
- [15] R. Meller, D. Boglu, G. K. Moortgat, STEP-HALOCSIDE/AFEAS Workshop, 23–25 March, Dublin, Ireland, 1993, p. 130–138.
- [16] S.R. Sellevåg, T. Kelly, H. Sidebottom, C.J. Nielsen, *Phys. Chem. Chem. Phys.* 6 (2004) 1243.
- [17] M.P. Sulbaek Andersen, M.D. Hurley, T.J. Wallington, J.C. Ball, J.W. Martin, D.A. Ellis, S.A. Mabury, O.J. Nielsen, *Chem. Phys. Lett.* 379 (2003) 28.
- [18] S. Pinnock, K.P. Shine, T.J. Smyth, M.D. Hurley, T.J. Wallington, *J. Geophys. Res.* 100 (1995) 23227.

- [19] T. Ando, *Z. Phys. B* 26 (1977) 263.
- [20] A. Zangwill, P. Soven, *Phys. Rev. A* 21 (1980) 156.
- [21] K. Nuroh, M.J. Stott, E. Zaremba, *Phys. Rev. Lett.* 49 (1982) 862.
- [22] G.D. Mahan, *J. Chem. Phys.* 76 (1982) 493.
- [23] S. Baroni, P. Giannozzi, A. Testa, *Phys. Rev. Lett.* 58 (1987) 1861.
- [24] Z.H. Levine, D.C. Allan, *Phys. Rev. Lett.* 63 (1989) 1719.
- [25] R. Bauernschmitt, R. Ahlrichs, *Chem. Phys. Lett.* 256 (1996) 454.
- [26] M.E. Casida, C. Jamorski, K.C. Casida, D.R. Salahub, *J. Chem. Phys.* 105 (1998) 4953.
- [27] M.E. Casida, C. Jamorski, K.C. Casida, D.R. Salahub, *J. Chem. Phys.* 108 (1998) 4439.
- [28] C. Jamorski, M.E. Casida, D.R. Salahub, *J. Chem. Phys.* 104 (1999) 5134.
- [29] M.E. Casida, D.R. Salahub, *J. Chem. Phys.* 113 (2000) 8918.
- [30] C. Adamo, G.E. Scuseria, V. Barone, *J. Chem. Phys.* 111 (1999) 2889.
- [31] K.B. Wiberg, R.E. Stratmann, M.J. Frisch, *Chem. Phys. Lett.* 297 (1998) 60.
- [32] Z.-L. Cai, J.R. Reimers, *J. Chem. Phys.* 112 (2000) 527.
- [33] S.J.A. van Gisbergen, J.A. Groeneveld, A. Rosa, J.G. Snijders, E.J. Baerends, *J. Phys. Chem. A* 103 (1999) 6835.
- [34] J.B. Foresman, M. Head-Gordon, J.A. Pople, M.J. Frisch, *J. Phys. Chem.* 96 (1992) 135.
- [35] N.N. Matsuzawa, A. Ishitani, D.A. Dixon, T. Uda, *J. Phys. Chem. A* 105 (2001) 4953;  
N.N. Matsuzawa, S. Mori, E. Yano, S. Okazaki, A. Ishitani, D.A. Dixon, *Proc. SPIE* 3999 (2000) 375;  
N.N. Matsuzawa, A. Ishitani, D.A. Dixon, T. Uda, *Proc. SPIE* 4345 (2001) 396.
- [36] R.L. Waterland, K.D. Dobbs, A.M. Rinehart, A.E. Feiring, R.C. Wheland, B.E. Smart, *J. Fluor. Chem.* 122 (2003) 37.
- [37] M.J. Frisch, G.W. Trucks, H.B. Schlegel, G.E. Scuseria, M.A. Robb, J.R. Cheeseman, J.A. Montgomery, Jr., T. Vreven, K.N. Kudin, J.C. Burant, J.M. Millam, S.S. Iyengar, J. Tomasi, V. Barone, B. Mennucci, M. Cossi, G. Scalmani, N. Rega, G.A. Petersson, H. Nakatsuji, M. Hada, M. Ehara, K. Toyota, R. Fukuda, J. Hasegawa, M. Ishida, T. Nakajima, Y. Honda, O. Kitao, H. Nakai, M. Klene, X. Li, J.E. Knox, H.P. Hratchian, J.B. Cross, C. Adamo, J. Jaramillo, R. Gomperts, R.E. Stratmann, O. Yazyev, A.J. Austin, R. Cammi, C. Pomelli, J.W. Ochterski, P.Y. Ayala, K. Morokuma, G.A. Voth, P. Salvador, J.J. Dannenberg, V.G. Zakrzewski, S. Dapprich, A.D. Daniels, M.C. Strain, O. Farkas, D.K. Malick, A.D. Rabuck, K. Raghavachari, J.B. Foresman, J.V. Ortiz, Q. Cui, A.G. Baboul, S. Clifford, J. Cioslowski, B.B. Stefanov, G. Liu, A. Liashenko, P. Piskorz, I. Komaromi, R.L. Martin, D.J. Fox, T. Keith, M.A. Al-Laham, C.Y. Peng, A. Nanayakkara, M. Challacombe, P.M.W. Gill, B. Johnson, W. Chen, M.W. Wong, C. Gonzalez, J.A. Pople, Gaussian 03, Revision B.05, Gaussian, Inc., Pittsburgh, PA, 2003.
- [38] A.D. Becke, *J. Chem. Phys.* 98 (1993) 5648.
- [39] C. Lee, W. Yang, R.G. Parr, *Phys. Rev. B* 37 (1988) 785.
- [40] N. Godbout, D.R. Salahub, J. Andzelm, E. Can. Wimmer, *J. Chem.* 70 (1992) 560.
- [41] M.E. Casida, in: D.P. Chong (Ed.), *Recent Advances Density Functional Theory Methods Part I*, World Scientific, Singapore, 1995.
- [42] T.H. Dunning, P.J. Hay, in: H.F. Schaefer, III (Ed.), *Methods of Electronic Structure Theory*, 3, Plenum Press, New York, 1977.
- [43] W.J.L. Hehre, L. Radom, P.V.R. Schleyer, J.A. Pople, *Ab Initio Molecular Orbital Theory*, John Wiley & Sons, New York, 1986.
- [44] A.P. Scott, L. Radom, *J. Phys. Chem.* 100 (1996) 16502.
- [45] A. Nölle, F. Pär. Meller, G.K. Moortgat, E.R. Roeth, R. Ruhnke, H. Keller-Rudek, *UV-vis Spectra of Atmospheric Constituents, DLRFDF (Deutsches Fernerkundungsdatenzentrum)*, 1998, ISBN 3-89100-030-8.
- [46] G.O. Pritchard, G.H. Miller, J.K. Foote, *Can. J. Chem.* 40 (1962) 1830.
- [47] W.B. DeMore, S.P. Sander, C.J. Howard, A.R. Ravishankara, D.M. Golden, C.E. Kolb, R.F. Hampson, M.J. Kurylo, M.J. Molina, in: *Chemical Kinetics and Photochemical Data for Use in Stratospheric Modeling, NASA Panel for Data Evaluation, Evaluation no. 10, Jet Propulsion Laboratory Publication 92-20, August 15, 1992*, p. 155.
- [48] D.C. Moule, A.D. Walsh, *Chem. Rev.* 75 (1) (1975) 67.
- [49] G.H. Dieke, G.B. Kistiakowski, *Phys. Rev.* 45 (1934) 4.
- [50] R.D. Martinez, A.A. Buitrago, N.W. Howell, C.H. Hearn, J.A. Joens, *Atmos. Environ. A* 26 (1992) 785.
- [51] B.J. Finlayson-Pitts, J.N. Pitts, Jr., in: *Atmospheric Chemistry*, John Wiley & Sons, Inc., New York, 1986, p. 110 (See Table 3.5).